

Net-proton number cumulant ratios as a function of beam energy from an expanding nonequilibrium chiral fluid

Christoph Herold¹,* Ayut Limphirat, and Poramin Saikham²

Center of Excellence in High Energy Physics and Astrophysics, Suranaree University of Technology, Nakhon Ratchasima 30000, Thailand

Marlene Nahrgang

SUBATECH UMR 6457, IMT Atlantique, Université de Nantes, IN2P3–Centre National de la Recherche Scientifique, 4 rue Alfred Kastler, Nantes 44307, France

Tom Reichert and Marcus Bleicher³†

Institut für Theoretische Physik, Goethe Universität Frankfurt, Max-von-Laue-Strasse 1, Frankfurt am Main 60438, Germany and Helmholtz Research Academy Hesse for FAIR, GSI Helmholtz Center for Heavy Ion Physics, Campus Frankfurt, Max-von-Laue-Strasse 12, Frankfurt 60438, Germany



(Received 10 May 2022; accepted 21 July 2022; published 3 August 2022)

The beam energy scan program at RHIC provides data on net-proton number fluctuations with the goal to detect the QCD critical end point and first-order phase transition. Interpreting these experimental signals requires a vital understanding of the interplay of critical phenomena and the nonequilibrium dynamics of the rapidly expanding fireball. We study these aspects with a fluid dynamic expansion coupled to the explicit propagation of the chiral order parameter σ via a Langevin equation. Assuming a σ -proton coupling through an effective proton mass, we relate cumulants of the order parameter and the net-proton number at freeze-out and obtain observable cumulant ratios as a function of beam energy. We emphasize the role of the nonequilibrium first-order phase transition where a mixed phase with gradual freeze-out can significantly alter the cumulants. We find that the presence of a critical end point is clearly visible in the cumulant ratios for a relatively wide range of center-of-mass energies.

DOI: [10.1103/PhysRevC.106.024901](https://doi.org/10.1103/PhysRevC.106.024901)

I. INTRODUCTION

Since the experimental discovery of a quark-gluon plasma created in high-energy heavy-ion collisions [1,2], uncovering the details of the phase diagram of quantum chromodynamics (QCD) has attracted considerable interest and our current knowledge is still limited. We know, however, from lattice QCD, that at small values of the baryochemical potential μ_B , the transition from hadronic matter to a phase of deconfinement and chiral symmetry restoration is a continuous crossover rather than an actual phase transition. For intermediate to large μ_B , lattice QCD is not directly applicable and we have to rely on alternative techniques which in many cases predict a critical end point (CEP) and adjacent first-order phase transition (FOPT). These different approaches

rely on functional methods [3,4] or low-energy effective models [5–7], and consequently yield a wide range of different results.

One characteristic signature of criticality is the nonmonotonic behavior of cumulants and cumulant ratios of conserved quantities [8–13] which generally exhibit maxima or minima at the T and μ_B values of the transition. Motivated by this idea, experimental collaborations have started programs to measure these in event-by-event fluctuations (see publications by STAR [14,15], NA49/61 [16,17], and HADES [18]). In the future, the facilities NICA [19] and FAIR [20] are going to investigate further by bridging the current gap in center-of-mass energies between STAR and HADES.

For a proper understanding of the dynamics of the fireball created in a heavy-ion collision, models have been developed to describe the nonequilibrium expansion and ultimately predict experimental observables related to a CEP [21–35] or FOPT [36–44]. Here, finite-size and finite-time effects influence the fluctuation observables like, e.g., the net-proton number cumulants that have an anomalous structure in the ratio of fourth to second cumulant with a strong enhancement above the Poisson baseline at the lowest center-of-mass energy of $\sqrt{s_{NN}} = 7.7$ GeV [15].

In the work reported here, we model the evolution of the plasma by a simple longitudinal Bjorken expansion along the

*herold@g.sut.ac.th

†Also at GSI Helmholtzzentrum für Schwerionenforschung GmbH, Planckstrasse 1, Darmstadt 64291, Germany.

Published by the American Physical Society under the terms of the [Creative Commons Attribution 4.0 International](https://creativecommons.org/licenses/by/4.0/) license. Further distribution of this work must maintain attribution to the author(s) and the published article's title, journal citation, and DOI. Funded by SCOAP³.

beam axis based on a chiral fluid dynamics model without spatial inhomogeneities [43]. The sigma field or chiral condensate as the order parameter is propagated via a Langevin equation of motion that couples to an expanding quark-antiquark fluid in local thermal equilibrium. We end the evolution as soon as it hits a parametrized freeze-out curve where we calculate net-proton number cumulants from cumulants of the sigma field by assuming a superposition of standard Poisson and critical fluctuations [24]. We correct our results by the effect of volume fluctuations as detailed in [45]. In this paper, we aim to reveal possible signatures in the net-proton number cumulants that would confirm or rule out a CEP and FOPT in strongly interacting matter.

After a brief model description in Sec. II, we present and interpret our results on the various net-proton number cumulant ratios as a function of beam energy in comparison to data from STAR and HADES in Sec. III, and conclude with a summary in Sec. IV.

II. MODEL DESCRIPTION

The model is based on the Lagrangian of the widely studied quark-meson model [5,6,46] with a CEP at $(T_{\text{CEP}}, \mu_{\text{CEP}}) = (100, 200)$ MeV. Although arguably simple, the model provides a description of a chiral phase diagram with the generic features of a crossover, CEP, and FOPT. Currently, there is no agreement within the theoretical physics community on where to find the CEP in the phase diagram [47], yet recent QCD-based calculations from functional renormalization group techniques [4,48] suggest a location similar to the one in the quark-meson model in mean field. We use the fluctuation of the sigma field as the critical mode of the QCD CEP, characterized by a vanishing sigma mass which has also provided one of the fundamental motivations for the beam energy scan program at RHIC [24,49].

Here and in the following, μ denotes the quark chemical potential, thus $\mu = \mu_B/3$. The Lagrangian for light quarks $q = (u, d)$ and the chiral order parameter σ with potential U reads

$$\mathcal{L} = \bar{q}(i\gamma^\mu \partial_\mu - g\sigma)q + \frac{1}{2}(\partial_\mu \sigma)^2 - U(\sigma), \quad (1)$$

$$U(\sigma) = \frac{\lambda^2}{4}(\sigma^2 - f_\pi^2)^2 - f_\pi m_\pi^2 \sigma + U_0, \quad (2)$$

with parameters $f_\pi = 93$ MeV, $m_\pi = 138$ MeV, and U_0 such that $U(\sigma) = 0$ in the ground state. The value of the pion fields has already been set to its vacuum expectation value of zero. The quark-sigma coupling constant g is fixed requiring that $3g\sigma$ equals the nucleon mass of 940 MeV in vacuum.

A. Equations of motion

We evolve the zero mode or volume-averaged sigma field defined as $\sigma(\tau) = \frac{1}{V} \int d^3x \sigma(\tau, x)$ using a Langevin equation of motion,

$$\ddot{\sigma} + \left(\frac{D}{\tau} + \eta\right)\dot{\sigma} + \frac{\delta\Omega}{\delta\sigma} = \xi, \quad (3)$$

neglecting spatial fluctuations. We describe the expanding fluid using a Bjorken model, and consequently use proper

time τ rather than coordinate time t , starting from an initial thermalization at $\tau_0 = 1$ fm. Consequently, the dots in Eq. (3) denote derivatives with respect to τ . For our case of purely longitudinal hydrodynamic flow, we set $D = 1$ in the Hubble term. The full and proper nonequilibrium dynamics of sigma is encoded in the dissipation coefficient η and the stochastic noise ξ which are related by a dissipation-fluctuation relation [50]:

$$\langle \xi(t)\xi(t') \rangle = \frac{m_\sigma \eta}{V} \coth\left(\frac{m_\sigma}{2T}\right) \delta(t - t'). \quad (4)$$

Here, ξ is assumed Gaussian and white, i.e., it is not correlated over time. The damping coefficient η includes effects from various intersigma and sigma-quark scattering processes (see [50] for further details about this model and the explicit derivation of the coupled equations of motion).

The quark-antiquark fluid is given by the ideal energy-momentum tensor $T_q^{\mu\nu} = (e + p)u^\mu u^\nu - pg^{\mu\nu}$. From the vanishing of its divergence, we obtain the equation for the energy density:

$$\dot{e} = -\frac{e + p}{\tau} + \left[\frac{\delta\Omega_{q\bar{q}}}{\delta\sigma} + \left(\frac{D}{\tau} + \eta\right)\dot{\sigma} \right] \dot{\sigma}. \quad (5)$$

The net-baryon density does not directly couple to σ and obeys the equation

$$\dot{n} = -\frac{n}{\tau}. \quad (6)$$

Note that the fireball volume which appears in Eq. (4) and also later in the description of the freeze-out cumulants is given by $V = \pi R^2 \tau$, with a gold nucleus radius of $R = 7.3$ fm, assuming central Au + Au collisions.

B. Freeze-out and mapping to beam energies

We investigate higher order cumulant ratios of the net-proton number along a freeze-out curve which has been obtained from thermal model fits to experimental data from SIS, AGS, SPS, and RHIC for a wide range of beam energies from $\sqrt{s} = 2.24$ to 200 A GeV [51]. The parametrization reads

$$T_{f.o.}(\mu_B) = a - b\mu_B^2 - c\mu_B^4, \quad (7)$$

with $a = 0.166$ GeV, $b = 0.139$ GeV⁻¹, and $c = 0.053$ GeV⁻³. To ensure that this freeze-out line is situated below the phase boundary of our underlying model, we rescale Eq. (7) such that $T_{f.o.}(\mu = 0)$ equals the crossover temperature at $\mu = 0$ that we have identified from a maximum in the quark-number susceptibilities.

Initial conditions are fixed by setting T_i and μ_i equal to the set of initial values chosen in a previous study [43] such that the evolutions will be able to probe crossover, CEP, and FOPT in the phase diagram. The point where the evolution of the fluid according to Eqs. (3), (5), and (6) meets the freeze-out curve for the first time is then used to map the initial condition to a corresponding beam energy via

$$\mu_B(\sqrt{s}) = \frac{d}{1 + e\sqrt{s}}, \quad (8)$$

with parameters $d = 1.308$ GeV and $e = 0.273$ GeV⁻¹ determined in accordance with the freeze-out curve above [51]. The baryochemical potential in Eq. (8) is obtained from averaging over events with the same initial condition. Note that the thus obtained beam energies are to be understood as guidelines to put our results into the context of experimentally obtained data from STAR and HADES. Even though in our present model the CEP is passed for evolutions with an initial $\sqrt{s} \approx 5$ GeV, this does not mean that we necessarily expect the physical CEP to be found there. However, it allows us to estimate the impact of a CEP on measurable observables in a fully dynamical nonequilibrium setup if it indeed exists in this low-energy range.

C. Sigma and net-proton number cumulants

To relate the fluctuations in the chiral order parameter σ to fluctuations or cumulants of the net-proton number, we follow the strategy outlined in [24]. Consider an infinitesimal change of the chiral field, $\delta\sigma$, leading to a change of the effective proton mass by $\delta m = g\delta\sigma$. Assuming a sigma-proton coupling $g\sigma\bar{p}p$, we may write fluctuations of the momentum space distribution function for protons, f_k , as

$$\delta f_k = \delta f_k^0 + \frac{\partial n_{\text{FD}}}{\partial m} g \delta\sigma. \quad (9)$$

The first term δf_k^0 is the purely statistical fluctuation, and in the second term n_{FD} denotes the Fermi-Dirac distribution for a particle of a given mass m . The fluctuation of the net-proton multiplicity $N = V d \int \frac{d^3k}{(2\pi)^3} f_k$ is then given by

$$\delta N = \delta N^0 + V g \delta\sigma d \int \frac{d^3k}{(2\pi)^3} \frac{\partial n_{\text{FD}}}{\partial m}, \quad (10)$$

where $d = 2$ is the spin degeneracy factor. The first term δN^0 can be assumed Poisson distributed, given that $n_p \ll 1$, i.e., effects from quantum statistics are negligible [24]. Consequently, all of its cumulants are equal to the expectation value $\langle N \rangle$. In leading order and assuming no correlations between δN^0 and $\delta\sigma$, we can express cumulants of order n as

$$\langle \delta N^n \rangle_c = \langle N \rangle + \langle \delta\sigma_V^n \rangle_c \left(g d \int \frac{d^3k}{(2\pi)^3} \frac{\partial n_{\text{FD}}}{\partial m} \right)^n. \quad (11)$$

In this notation, $\sigma_V = \int d^3x \sigma = \sigma V$ as we neglect spatial fluctuations, and $\langle \cdot \rangle_c$ is the respective cumulant, which is equal to the expectation value for $n = 1$ and to the corresponding central moment for $n = 2, 3$. For $n = 4$, we have

$$\langle \delta\sigma_V^4 \rangle_c = \langle \delta\sigma_V^4 \rangle - 3 \langle \delta\sigma_V^2 \rangle^2, \quad (12)$$

and similarly for $\langle \delta N^n \rangle_c$. In Sec. III, we will use the shorter notation C_n for the net-proton number cumulants $\langle \delta N^n \rangle_c$ which has also been commonly used in experimental studies of recent years.

III. RESEARCH PROCEDURE AND RESULTS

We initialize the fluid at a set of fixed values (T_i, μ_i) and define initial sigma field, energy density, quark number density, and pressure as the corresponding equilibrium values.

The pairs of initial values are hereby adopted from earlier works [43,52] and will be matched to center-of-mass energies using the freeze-out condition, Eq. (8). The coupled system evolves according to the equations of motion until the freeze-out curve is hit. Notably, for expansions at high baryochemical potential, the freeze-out curve can be hit more than once due to the nonequilibrium evolution of the expanding plasma. This effect occurs due to the sudden release in latent heat that drives the system back into the chirally symmetric phase, visible in a back-bending of the trajectories in T and μ [40,43]. In contrast to that, an equilibrated hydrodynamic system with constant S/A would pass along the phase boundary for a finite amount of time [53]. To take into account this effect of a possible mixed phase in a heavy-ion collision and its impact on the observed cumulants, we evolve the system for these cases until a second crossing of the freeze-out curve and subsequently calculate cumulants at both crossing or hit points. In the following figures and text, we consequently refer to the “first hit” as the cumulants evaluated at the first crossing of the freeze-out line and the “second hit” as those evaluated at the second crossing, where applicable. This is relevant for evolutions near the CEP in the phase diagram or crossing the FOPT line [52]. Ultimately, it will provide us with a range of possible cumulants for the respective energies. The characteristic back-bending after passing the phase boundary becomes most pronounced for evolutions passing the FOPT due to significant energy dissipation pushing the system back into the chirally restored phase. Physically, this process could manifest in a gradual freeze-out where the medium undergoes droplet formation [37,54]. Another suggested signal for such a delayed transition process is an enhancement in the dilepton production [55].

We simulate 10^7 events and calculate event-by-event fluctuations in terms of cumulants of σ_V . Since these are subject to significant fluctuations of the freeze-out volume, we include the corresponding corrections as derived in [45]. This is most relevant for evolutions at the lowest energies with large variations in the time at which different events from the same initial condition hit the freeze-out curve [52]. Equation (11) allows us to determine the net-proton number cumulants. The such obtained values are compared with a Poisson baseline. For the net-proton number ($p - \bar{p}$), the cumulants assuming Poisson distributed proton and antiproton numbers are calculated by

$$C_{n,p-\bar{p}} = C_{n,p} + (-1)^n C_{n,\bar{p}}, \quad (13)$$

where $C_{n,p}$, $C_{n,\bar{p}}$ are equal to the expectation values of the Poisson distribution for all orders n (see [15]). We furthermore provide comparison to the equilibrium net-baryon number susceptibilities which are obtained as

$$\chi_n = \frac{\partial^n (p/T^4)}{\partial (\mu_B/T)^n}. \quad (14)$$

Figure 1 (top) shows the ratio C_2/C_1 of the net-proton number compared to results from STAR for energies $\sqrt{s_{\text{NN}}} \geq 7.7$ GeV [15] and HADES for $\sqrt{s_{\text{NN}}} = 2.4$ GeV [18]. Since the HADES collaboration reported a strong dependence of cumulant ratios on the chosen rapidity window, we depict results for both $|y| < 0.4$ and 0.5 for comparison, the latter one also being applied to STAR data. In [18], a reliable rapidity

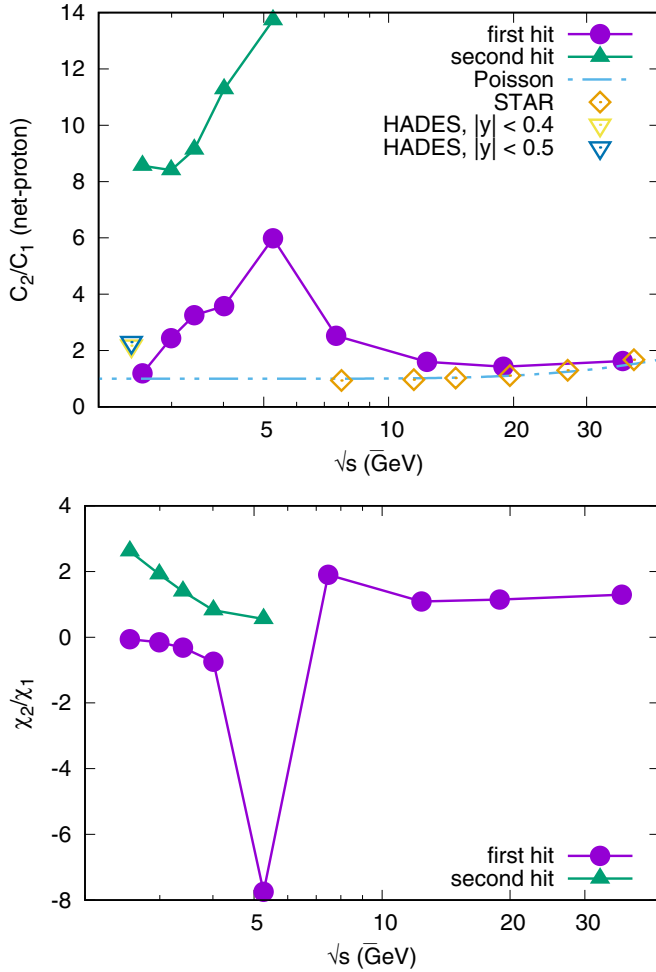


FIG. 1. Cumulant ratio C_2/C_1 of the net-proton number compared to results from STAR [15] and HADES [18] (top). Susceptibility ratio for comparison shows an extremum at the same center-of-mass energy (bottom).

window of $|y| < 0.46$ is quoted. We see that for high energies our results together with STAR data lie close to the Poisson baseline. With decreasing energy, our model yields values that are gradually enhanced until they reach a maximum at around 5 GeV for the evolution that passes through or close by the CEP and freezes out close to a spinodal line of the FOPT [52]. Along the spinodal lines, all susceptibilities diverge in nonequilibrium with critical exponents that become larger with order of the susceptibility [41,56]. This is clearly reflected in the peak of the corresponding susceptibility ratio visible on the bottom of Fig. 1. Further lowering the energy results in a gradual return to the baseline for the first hit of the freeze-out curve, while for the second hit significantly larger fluctuations are observed, possibly due to an enhancement of spinodal instabilities. Notably, the data from HADES lie within the thus obtained range of cumulant ratios at the lowest beam energy. Since our model is arguably simplistic, the comparison to experimental data must be understood as qualitative, at best. The quark-meson model contains only a small number of degrees of freedom, especially in the hadronic

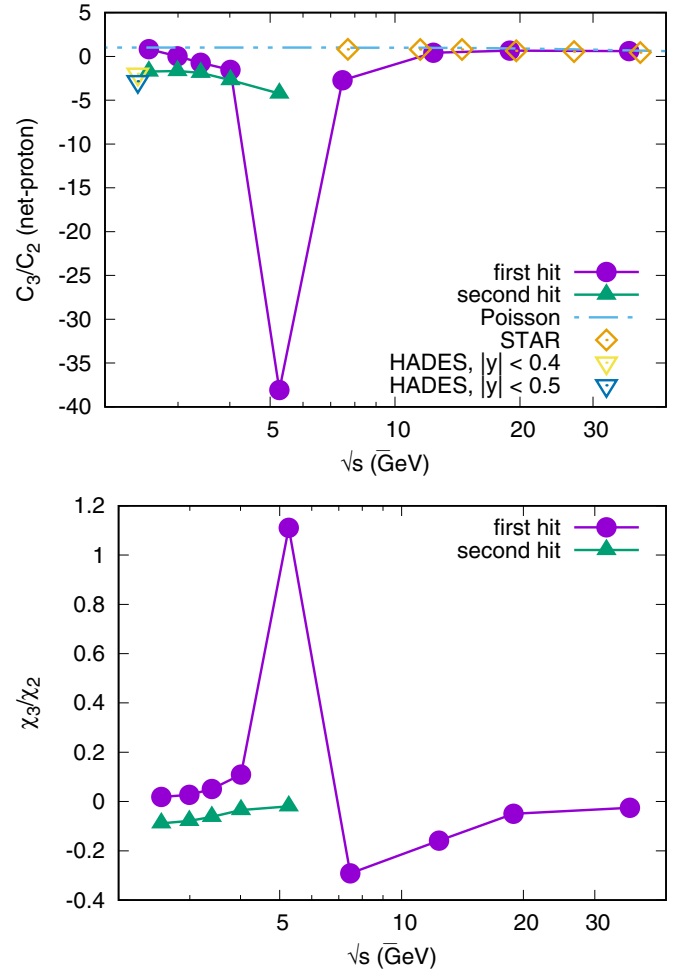


FIG. 2. Cumulant ratio C_3/C_2 of the net-proton number compared to results from STAR [15] and HADES [18] (top). Susceptibility ratio for comparison shows an extremum at the same center-of-mass energy (bottom).

sector, and it has been known that its equation of state behaves unphysically for low temperatures [57]. Obviously, a significant gap in the experimental data will have to be filled by future experiments such as FAIR and NICA that aim at exploring the high- μ_B region of the QCD phase diagram. The susceptibility ratio on the right hand side of Fig. 1 shows a similar trend for high energies. The freeze-out close to the spinodal line, where susceptibilities in the presence of spinodal instabilities diverge and change sign [41,56], results in the strongly negative value of χ_2/χ_1 which is reflected in the peak of C_2/C_1 , similar to what we found for the other cumulant ratios as we will discuss below.

The cumulant ratio C_3/C_2 is shown and compared to experimental data in Fig. 2 (top). The most notable feature is, again, the strong impact of the CEP around $\sqrt{s} = 5$ GeV. Besides that, the obtained points from our model are close to the baseline for high energies and the second hit at the lowest energy is close to the data point from HADES, where a suppression of C_3/C_2 was found, possibly a result of the dynamics at the FOPT. Once again, a quantitative comparison

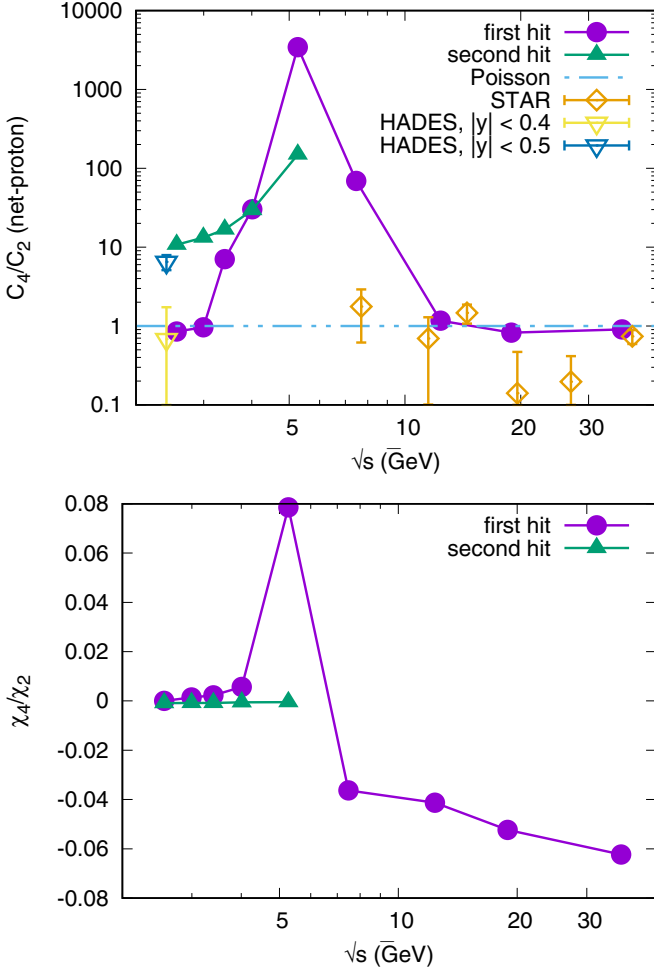


FIG. 3. Cumulant ratio C_4/C_2 of the net-proton number compared to results from STAR [15] and HADES [18] (top). Susceptibility ratio for comparison shows a maximum at the same center-of-mass energy (bottom).

between our model results and the experimental data is not intended here and its inclusion is made for the sake of improving our qualitative understanding of the measured cumulant ratios in the context of a nonequilibrium FOPT and CEP. The net-baryon number susceptibility ratio on the bottom part of the same figure approaches zero for the first hit and remains negative for the second hit of the parametrized freeze-out curve. The most apparent difference to C_3/C_2 is the sign at the CEP evolution which is positive for the susceptibilities, but negative for the cumulants. As mentioned before, the evolution passing close to the CEP freezes out very close to the spinodal line where some of the susceptibilities change sign [41]. Therefore, finite-time effects can here dramatically influence the final values at freeze-out.

Finally, the ratio C_4/C_2 is depicted in Fig. 3; on the top we see qualitative similarities between our model results and the experimental data. A slight suppression in the STAR data around 20 GeV is also present in our model calculations where the cumulant ratio lies below the Poisson baseline, although with smaller significance. Then, as the beam

energy is lowered, the notable point at 7.7 GeV where C_4/C_2 is enhanced is reflected in an enhancement, albeit orders of magnitude larger, of the ratio from our calculation. Here, it is necessary to emphasize that the aforementioned freeze-out near the spinodal line leads to larger and larger cumulants at higher orders. Lowering the beam energy even further, our calculations approach the HADES results which for this cumulant ratio show the strongest dependence on the applied experimental cut. Within error bars, both points lie within our range defined by the first and second hit of $C_4/C_2 \approx 1-10$. The susceptibility ratios, shown on the bottom of the same figure, are close to zero at these low energies which could indicate that an enhancement of the net-proton number cumulants occurs through a prolonged evolution in the mixed-phase region for the FOPT. The positive peak for the CEP evolution is also found in the susceptibilities; however, for larger energies, the values are slightly negative, which is only partly reflected in the obtained cumulants.

IV. SUMMARY AND CONCLUSIONS

We have studied cumulant ratios C_2/C_1 , C_3/C_2 , and C_4/C_2 of the net-proton number at STAR and HADES energies within a nonequilibrium chiral Bjorken expansion. Here, a sigma model served as input for a generic chiral phase structure and net-proton cumulants have been calculated event by event from cumulants of the sigma field at a parametrized freeze-out curve. Volume fluctuations have been accounted for and were properly corrected. Although admittedly crude and neglecting effects of an inhomogeneous medium, the dynamical description nevertheless shows some qualitative resemblance to the experimental data, in the approach of the Poisson baseline for high energies far away from the critical region, but also the enhancement or suppression of certain cumulant ratios at a speculated CEP or FOPT. We have demonstrated the general impact of a CEP and FOPT on cumulant ratios as key observables for probing the QCD phase structure. If indeed a CEP is present for center-of-mass energies below 7.7 GeV, it should be clearly visible in a relatively wide energy range and manifest itself and the adjacent FOPT through an enhancement and/or suppression of cumulant ratios. Clearly, the current gap in beam energies from 2.4 to 7.7 GeV requires filling by future experiments.

Possible future improvements of our current model include the consideration of a spatially inhomogeneous fluid and an extension of the study to full (3 + 1) dimensional hydrodynamics.

ACKNOWLEDGMENTS

This work was supported by Suranaree University of Technology, by Thailand Science Research and Innovation, and by National Science Research and Innovation Fund (NSRF) Project No. 160355. This research has received funding support from NSRF via the Program Management Unit for Human Resources and Institutional Development, Research and Innovation (Grant No. B16F640076).

- [1] U. W. Heinz and M. Jacob, 2000 (unpublished).
- [2] J. Adams, Jr. *et al.* (STAR), *Nucl. Phys. A* **757**, 102 (2005).
- [3] C. S. Fischer, J. Luecker, and C. A. Welzbacher, *Phys. Rev. D* **90**, 034022 (2014).
- [4] F. Gao and J. M. Pawlowski, *Phys. Lett. B* **820**, 136584 (2021).
- [5] O. Scavenius, A. Mocsy, I. N. Mishustin, and D. H. Rischke, *Phys. Rev. C* **64**, 045202 (2001).
- [6] B.-J. Schaefer and J. Wambach, *Nucl. Phys. A* **757**, 479 (2005).
- [7] K. Fukushima, *Phys. Rev. D* **77**, 114028 (2008).
- [8] F. Karsch, *J. Phys.: Conf. Ser.* **779**, 012015 (2017).
- [9] A. Bazavov, D. Bollweg, H. T. Ding, P. Enns, J. Goswami, P. Hegde, O. Kaczmarek, F. Karsch, R. Larsen, S. Mukherjee, H. Ohno, P. Petreczky, C. Schmidt, S. Sharma, and P. Steinbrecher, *Phys. Rev. D* **101**, 074502 (2020).
- [10] V. Skokov, B. Friman, and K. Redlich, *Phys. Rev. C* **83**, 054904 (2011).
- [11] G. A. Almasi, B. Friman, and K. Redlich, *Phys. Rev. D* **96**, 014027 (2017).
- [12] R. Wen, C. Huang, and W.-J. Fu, *Phys. Rev. D* **99**, 094019 (2019).
- [13] P. Isserstedt, M. Buballa, C. S. Fischer, and P. J. Gunkel, *Phys. Rev. D* **100**, 074011 (2019).
- [14] X. Luo and N. Xu, *Nucl. Sci. Tech.* **28**, 112 (2017).
- [15] M. Abdallah *et al.* (STAR), *Phys. Rev. C* **104**, 024902 (2021).
- [16] K. Grebieszkow (NA49 Collaboration), *Nucl. Phys. A* **830**, 547C (2009).
- [17] E. Andronov (NA61/SHINE), *Nucl. Phys. A* **982**, 835 (2019).
- [18] J. Adamczewski-Musch *et al.* (HADES), *Phys. Rev. C* **102**, 024914 (2020).
- [19] theor.jinr.ru/twiki/cgi/view/NICA/NICAWHITEPAPER.
- [20] B. Friman, C. Hohne, J. Knoll, S. Leupold, J. Randrup *et al.*, *Lect. Notes Phys.* **814**, 1 (2011).
- [21] B. Berdnikov and K. Rajagopal, *Phys. Rev. D* **61**, 105017 (2000).
- [22] C. Athanasiou, K. Rajagopal, and M. Stephanov, *Phys. Rev. D* **82**, 074008 (2010).
- [23] M. Nahrgang, S. Leupold, and M. Bleicher, *Phys. Lett. B* **711**, 109 (2012).
- [24] M. A. Stephanov, *Phys. Rev. Lett.* **107**, 052301 (2011).
- [25] C. Herold, M. Nahrgang, I. N. Mishustin, and M. Bleicher, *Phys. Rev. C* **87**, 014907 (2013).
- [26] S. Mukherjee, R. Venugopalan, and Y. Yin, *Phys. Rev. C* **92**, 034912 (2015).
- [27] L. Jiang, P. Li, and H. Song, *Nucl. Phys. A* **956**, 360 (2016).
- [28] L. Jiang, P. Li, and H. Song, *Phys. Rev. C* **94**, 024918 (2016).
- [29] C. Herold, M. Nahrgang, Y. Yan, and C. Kobdaj, *Phys. Rev. C* **93**, 021902(R) (2016).
- [30] C. Herold, M. Bleicher, M. Nahrgang, J. Steinheimer, A. Limphirat, C. Kobdaj, and Y. Yan, *Eur. Phys. J. A* **54**, 19 (2018).
- [31] M. Stephanov and Y. Yin, *Phys. Rev. D* **98**, 036006 (2018).
- [32] M. Stephanov and Y. Yin, *Nucl. Phys. A* **967**, 876 (2017).
- [33] M. Nahrgang, M. Bluhm, T. Schafer, and S. A. Bass, *Phys. Rev. D* **99**, 116015 (2019).
- [34] M. Nahrgang and M. Bluhm, *Phys. Rev. D* **102**, 094017 (2020).
- [35] L. Du, U. Heinz, K. Rajagopal, and Y. Yin, *Phys. Rev. C* **102**, 054911 (2020).
- [36] L. P. Csernai and J. I. Kapusta, *Phys. Rev. Lett.* **69**, 737 (1992).
- [37] J. Randrup, *Phys. Rev. C* **79**, 054911 (2009).
- [38] J. Randrup, *Phys. Rev. C* **82**, 034902 (2010).
- [39] J. Steinheimer and J. Randrup, *Phys. Rev. Lett.* **109**, 212301 (2012).
- [40] C. Herold, M. Nahrgang, I. Mishustin, and M. Bleicher, *Nucl. Phys. A* **925**, 14 (2014).
- [41] C. Herold, M. Nahrgang, Y. Yan, and C. Kobdaj, *J. Phys. G* **41**, 115106 (2014).
- [42] L. Jiang, S. Wu, and H. Song, *EPJ Web Conf.* **171**, 16003 (2018).
- [43] C. Herold, A. Kittiratpattana, C. Kobdaj, A. Limphirat, Y. Yan, M. Nahrgang, J. Steinheimer, and M. Bleicher, *Phys. Lett. B* **790**, 557 (2019).
- [44] R. V. Poberezhnyuk, O. Savchuk, M. I. Gorenstein, V. Vovchenko, and H. Stoecker, *Phys. Rev. C* **103**, 024912 (2021).
- [45] V. Skokov, B. Friman, and K. Redlich, *Phys. Rev. C* **88**, 034911 (2013).
- [46] A. Mocsy, I. N. Mishustin, and P. J. Ellis, *Phys. Rev. C* **70**, 015204 (2004).
- [47] A. Pandav, D. Mallick, and B. Mohanty, 2022 (unpublished).
- [48] W.-j. Fu, J. M. Pawlowski, and F. Rennecke, *Phys. Rev. D* **101**, 054032 (2020).
- [49] X. Luo (STAR), PoS **CPOD2014**, 019 (2015).
- [50] M. Nahrgang, S. Leupold, C. Herold, and M. Bleicher, *Phys. Rev. C* **84**, 024912 (2011).
- [51] J. Cleymans, H. Oeschler, K. Redlich, and S. Wheaton, *Phys. Rev. C* **73**, 034905 (2006).
- [52] C. Herold, A. Limphirat, P. Saikham, and M. Nahrgang, *Phys. Scr.* **97**, 064001 (2022).
- [53] J. Steinheimer, M. Bleicher, H. Petersen, S. Schramm, H. Stocker, and D. Zschesche, *Phys. Rev. C* **77**, 034901 (2008).
- [54] I. N. Mishustin, *Phys. Rev. Lett.* **82**, 4779 (1999).
- [55] F. Seck, T. Galatyuk, A. Mukherjee, R. Rapp, J. Steinheimer, and J. Stroth, [arXiv:2010.04614](https://arxiv.org/abs/2010.04614) (2020).
- [56] C. Sasaki, B. Friman, and K. Redlich, *Phys. Rev. D* **77**, 034024 (2008).
- [57] J. Steinheimer, J. Randrup, and V. Koch, *Phys. Rev. C* **89**, 034901 (2014).